Marginally-Stable Thermal Equilibria of Rayleigh-Bénard Convection

Liam O'Connor[1], Daniel Lecoanet[1,2], and Evan Anders[2]
[1] *Department of Engineering Sciences and Applied Mathematics, Northwestern University, Evanston, IL 60208 USA and*
[2] *Center for Interdisciplinary Exploration and Research in Astrophysics, Northwestern University, Evanston, IL, 60201 USA*

Natural convection is ubiquitous throughout the physical sciences and engineering, yet many of its important properties remain elusive – particularly in the large Rayleigh number regime. In this investigation, we derive and solve a quasilinear form of the Boussinesq Rayleigh-Bénard equations. Eigenfunction amplitudes are obtained by requiring marginal-stability. We obtain symmetric thermally-equilibrated solutions and analyze their properties. Solutions to the quasilinear problem differ from statistically-steady 2-dimensional Rayleigh-Beńard convection simulation data, having thinner boundary layers and larger Nusselt numbers Nu which scale like $\mathrm{Nu} \sim Ra^{1/3}$. We initialize 2-dimensional simulations with solutions to the quasilinear problem; they do not undergo a convective transient period and are kinetically exaggerated.

I. INTRODUCTION

Rayleigh-Bénard convection plays a foundational role in large-scale astrophysical and geophysical settings. Buoyancy-driven convection regulates heat transfer and often gives way to violently turbulent flows, thereby dominating large-scale behaviors and fueling small-scale processes in important systems [1].

Aggressive convection, which is associated with large Rayleigh numbers Ra, is difficult to simulate. State of the art convection simulations performed by [2] have reached $Ra \sim 10^{14}$ but estimates for stars are $Ra \sim 10^{20}$ [3]. The scaling behavior of the Nusselt number $\mathrm{Nu} \sim Ra^{\beta}$ in the asymptotic ultimate regime is of particular interest. There exists a substantial body of work pertaining to this specific topic with no general consensus [4–10].

Reduced models are particularly useful in this context because they allow us to study the problem with relatively low expense. Much of the published work on this topic relates to unstable exact coherent states (ECS) [11–14]. Simulations and analysis performed by [15, 16] suggest that chaotic simulation trajectories can be represented by a Markov chain whose long-term behavior is given by the time-weighted-average of a finite set of ECS. Should that be the case, it is crucial that we discover and classify such states.

In [17], researchers compute ECS in parallel shear flows by deriving and solving a quasilinear formulation of the Navier-Stokes equations via multi-scale asymptotic arguments. This is realized by defining a mean state which, hypothetically, evolves on a slow time-scale. Marginal stability is required at each successive timestep to constrain the perturbation amplitudes. A similar strategy is employed by [18], where an analytic expression for the first-order perturbations' amplitude is found by deriving a solvability condition of the second-order perturbations and integrating over the domain spatially. We seek to solve the Boussinesq Rayleigh–Bénard convection equations using an analogous strategy. The application of this procedure yields time-invariant solutions to the quasilinear problem with a range of expected and unexpected features.

II. MODEL SETUP

We begin with the non-dimensionalized Boussinesq approximation for Rayleigh-Bénard Convection. The domain $\mathcal{D}$ is 2-dimensional rectangular and horizontally periodic with spatial dimensions $0 < x < 4$ and $-1/2 < z < 1/2$. The fluid of interest is constrained between two planar boundaries at $z = -1/2$ and $z = 1/2$ with fixed temperatures 1 and 0 respectively. At both boundaries we specify impenetrable, no-slip conditions, such that the velocity $\mathbf{u} = u\hat{x} + w\hat{z} = \mathbf{0}$ at $z = \pm 1/2$. The equations of motion are then given by

$$\nabla \cdot \mathbf{u} = 0 \tag{1}$$

$$\frac{\partial \mathbf{u}}{\partial t} + \mathbf{u} \cdot \nabla \mathbf{u} = -\nabla p + T\hat{z} + \mathcal{R}\nabla^2 \mathbf{u} \tag{2}$$

$$\frac{\partial T}{\partial t} + \mathbf{u} \cdot \nabla T = \mathcal{P}\nabla^2 T \tag{3}$$

where p is pressure and T is temperature. For completeness, we specify a final boundary condition $p = p_0$ at $z = \pm 1/2$. Any system of this form can be characterized by its dimensionless Rayleigh number $Ra = \frac{g\alpha L^3 \Delta T}{\nu\kappa}$ and Prandtl number $Pr = \frac{\nu}{\kappa}$, where g, α, L, $\Delta T, \nu, \kappa$ are the gravitational acceleration, coefficient of thermal expansion, domain height, boundary temperature difference, kinematic viscosity, and thermal diffusivity respectively. For convenience, we define

$$\mathcal{R} = \sqrt{\frac{Pr}{Ra}}, \qquad \mathcal{P} = \frac{1}{\sqrt{PrRa}}. \tag{4}$$

To derive the quasilinear form, we posit that an arbitrary field f can be represented as the sum of a mean profile (denoted by $\bar{f}$) and a perturbation function (de-

noted by f').

$$\mathbf{u}(x,z,t) = A(t)\mathbf{u}'(x,z,t) \tag{5}$$
$$= A(t)u'(x,z,t)\hat{x} + A(t)w'(x,z,t)\hat{z} \tag{6}$$
$$T(x,z,t) = \bar{T}(z,t) + A(t)T'(x,z,t) \tag{7}$$
$$p(x,z,t) = \bar{p}(z,t) + A(t)p'(x,z,t). \tag{8}$$

where $A(t)$ is some unknown real amplitude and the mean-velocity components vanish due to incompressibility and symmetry. Perturbations must admit no horizontal-average; an arbitrary perturbation f' obeys

$$\langle f'(x,z,t)\rangle_x \equiv \int_0^4 f'(x,z,t)dx = 0. \tag{9}$$

Assuming the existance of nontrivial solutions, we also fix the volume-average over the entire domain

$$\langle T'^2\rangle_{\mathcal{D}} = 1 \tag{10}$$

thereby alleviating any ambiguity in $A(t)$. Substituting (7) into (3) and taking the horizontal average reduces the system to a simple initial value problem (IVP) for $\bar{T}$

$$\frac{\partial \bar{T}}{\partial t} + A^2\langle w'T'\rangle_x = \mathcal{P}\frac{\partial^2 \bar{T}}{\partial z^2}, \tag{11}$$

with associated boundary conditions $\bar{T}(-1/2,t) = 1$ and $\bar{T}(1/2,t) = 0$. It should be noted that we could obtain a similar IVP for u by breaking symmetry and considering some nontrivial mean horizontal flow $\bar{u}(z,t)$. However we must have $\bar{w}(z,t) = 0$ due to incompressibility.

To solve (11) numerically, we need the perturbations and their associated amplitude function $A(t)$. The former is obtained by solving the linearized system. Substituting (5)–(8) into (1)–(3) and subtracting (11) from the resulting temperature equation gives

$$\nabla\cdot\mathbf{u}' = 0 \tag{12}$$
$$\frac{\partial \mathbf{u}'}{\partial t} = -\nabla p' + T'\hat{z} + \mathcal{R}\nabla^2\mathbf{u}' \tag{13}$$
$$\frac{\partial T'}{\partial t} + \frac{\partial \bar{T}}{\partial z}w' = \mathcal{P}\nabla^2 T' \tag{14}$$

with Dirichlet boundary conditions

$$T'|_{z=\pm\frac{1}{2}} = 0, \quad u'|_{z=\pm\frac{1}{2}} = 0, \quad p'|_{z=\pm\frac{1}{2}} = 0. \tag{15}$$

In 1916, Lord Rayleigh observed that (12) and (14) can be manipulated into a separable form with generalized solutions

$$w'(x,z,t) = W(z)\,e^{i(k_x x - st)} \tag{16}$$
$$u'(x,z,t) = U(z)\,e^{i(k_x x - st)} \tag{17}$$
$$T'(x,z,t) = \theta(z)\,e^{i(k_x x - st)} \tag{18}$$
$$p'(x,z,t) = P(z)\,e^{i(k_x x - st)} \tag{19}$$

where $s = \sigma + i\omega$ and k_x is constrained, by periodicity, to the countably infinite set (spectrum) of wavenumbers

$$k_x \in \Big\{\frac{n\pi}{2}\,\Big|\, n\in\mathbb{N}\Big\}. \tag{20}$$

For each k_x, we can assess the stability of the perturbations by solving for the eigenvalue s, whose imaginary component ω plays the role of an exponential growth rate. Solution yields a finite set of eigenvalues, among which, that with maximum ω is assumed to be dominant. Positive eigenvalues indicate that the system is unstable to small disturbances of wavenumber k_x, while negative eigenvalues indicate stability. A complete linear stability analysis requires solution over the full spectrum of wavenumbers. The prototypical case is used to demonstrate that the critical Rayleigh number $Ra_c = 1708$ when $\frac{\partial \bar{T}}{\partial z} = -1$.

At some arbitrary time t_0, the forcing term $\langle w'T'\rangle_x$ can be found by solving an eigenvalue problem (EVP) which itself involves $\frac{\partial \bar{T}}{\partial z}$. We also assume this term is composed of eigenfunctions belonging to the dominant mode(s).

III. PERTURBATION EVOLUTION

Solving the linearized system (12) – (14) does not yield $A(t)$. To evolve $\bar{T}$, we assume the perturbations and mean quantities evolve according to different time-scales, as in [18]. Stable modes decay away rapidly. Unstable modes will not persist on the slow time-scale because the advective term $\langle w'T'\rangle_x$ tends to tends to stabilize $\bar{T}$, thereby creating a negative feedback loop. Only marginally stable modes can traverse this hypothetical time-scale separation. Therefore the amplitude function $A(t)$ must satisfy

$$\max_{k_x}\{\omega\} = 0. \tag{21}$$

For various Ra and fixed $Pr = 1$, we seek symmetric marginally-stable thermal equilibria (MSTE) $\bar{T}_{\mathrm{MSTE}}$, thereby satisfying $\frac{\partial \bar{T}}{\partial t} = 0$ according to (11). We employ the `Dedalus` pseudo-spectral python framework to solve the EVP outlined in Section II as well as the IVP (11) by representing each field with a dealiased Chebyshev polynomial basis. The necessary number of basis functions varies, as eigenfunctions and temperature profiles associated with large Ra admit increasingly small-scale features. We supplement `Dedalus` with the `Eigentools` package to compute $\langle w'T'\rangle_x$.

At $t = 0$, we begin with a marginally-stable initial profile $\bar{T}(z,0)$ whose construction is outlined in VI A. At some arbitrary time $t = t_0$, we seek to evolve $\bar{T}(z,t_0)$ into a new marginally-stable profile $\bar{T}(z,t_0+\Delta t)$ according to (11) using forward-Euler. This generally involves a unique and unknown value $A^2(t_0) > 0$. Our method of finding $A^2(t_0)$ is best illustrated through example.

An iteration is performed as follows: diffusing a marginally-stable temperature profile $\bar{T}(z,t_0)$ tends to

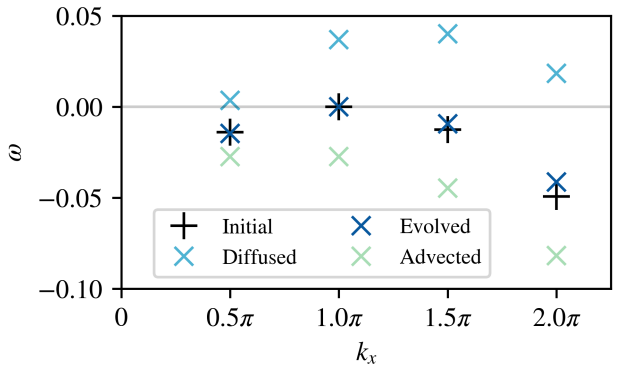

FIG. 1. Eigenvalue spectra for $Ra = 10^5$. The spectrum of an "initial" marginally-stable mean temperature profile $\bar{T}(z, t_0)$ has a maximum eigenvalue of 0. Given a small fixed timestep Δt, diffusion destabilizes the system, increasing its eigenvalues. Advection tends to stabilize the system, decreasing its eigenvalues. It follows that there exists some proportion $(A^2(t_0))$ of these two terms which yields a new marginally-stable mean temperature profile $\bar{T}(z, t_0+\Delta t)$, whose spectrum is "evolved".

increase its eigenvalues. Ignoring the diffusive term and evolving according to advection tends the stabilize the system. The appropriate amplitude $A^2(t_0)$ can then be approximated by

$$A^2(t_0) \sim -\frac{\omega_{\text{diff}}}{\omega_{\text{adv}}} \tag{22}$$

where ω_{diff} and ω_{adv} refer to the diffused and advected eigenvalues of the initially marginal mode (corresponding to the light blue and green points respectively at $k_x = \pi$ in Figure 1). $\bar{T}(z, t)$ is then evolved according to (11) and another eigenvalue solve is performed. Given a fixed timestep Δt, we assume the dominant eigenvalue can be described by a continuous function $\omega_{\max}(A^2)$ which is locally differentiable. We use Newton's method to find an amplitude which satisfies our marginal stability tolerance criterion $|\omega_{\max}(A^2)| \leq 10^{-9}$. The dominant mode is not fixed; an iteration can facilitate the transfer of marginal-stability from one mode to another. In section III A we specify procedures for the treatment of multiple simultaneously marginal modes.

A. Treatment of multiple marginally-stable modes

In most cases, we eventually encounter eigenvalue spectra with multiple simultaneously marginal modes. If ignored, we are forced to reduce the timestep and allow the modes to alternate. Instead, we generalize the advective term in (11) to accommodate N simultaneously marginal modes

$$A^2\langle w'b'\rangle_x = \sum_{n=1}^{N} A_n^2 \langle w'b'\rangle_{x,n} \tag{23}$$

where $\langle w'b'\rangle_{x,n}$ is composed of perturbations associated with $k_x = \frac{n\pi}{2}$. There are now N amplitudes to solve for and N eigenvalues to keep marginally-stable. In general, we expect a function $\omega : \mathbb{R}^N \to \mathbb{R}^N$ to have isolated roots (should they exist). We employ Broyden's method for root-finding in multi-dimensional functions whose derivatives are not explicitly known. Difficulty arises when transitioning between different numbers of marginal modes. Here we rely on $A^2 > 0$ by asserting that a mode which is *close enough* to marginal-stability can be included in the iteration provided that its respective amplitude is positive. Should we converge upon a negative amplitude, that mode is discarded and the iteration is repeated. In general we find that no other obvious course of action yields equilibria.

IV. PROPERTIES OF THERMALLY EQUILIBRATED STATES

MSTE are solutions to the quasilinear form of the Rayleigh-Bénard convection equations derived in section II. For this investigation, we calculate solutions for Ra in the range $10^5 - 10^9$. Their mean temperatures $\bar{T}_{\text{MSTE}}$ are symmetric about $z = 0$ by construction.

Figure 2 gives temperature profiles for $Ra = 10^8$ where the initial profile, given by (29), is employed at iteration 0; the MSTE profile corresponds to the thermally relaxed state; and the DNS (direct numerical simulations) profile is obtained by solving (1)–(3) with `Dedalus`, followed by horizontal and time averaging. The DNS curve is more diffuse than the MSTE curve, which in turn, is more diffuse than the initial curve. Performing an eigenvalue solve by setting $\bar{T}$ equal to the DNS profile yields positive eigenvalues. Comprehensively, this suggests that MSTE might maximize boundary layer thickness, while subject to the marginal stability constraint.

The most resilient and unexpected feature of thermally equilibrated mean temperature profiles are the pronounced dips adjacent to the boundary layers. These dips appear in every solution, regardless of Ra. Physically, they correspond to thin layers in which the temperature gradient reverses, contradicting an important hypothesis of [4]. This counter-diffusion, which opposes overall heat transfer, is overcome by the coinciding advective flux, shown in Figure 4.

Equilibrated states exhibit distinct behaviors for large and small Ra. This contrast is illustrated in Figure 4, where we give heat flux profiles and eigenvalue spectra for two cases: $Ra = 2 \times 10^5$ and $Ra = 10^9$. For lower Ra, there is a single presumed local maximum in the eigenvalue spectrum, whose adjacent modes' advection profiles occupy the bulk of the domain. These states have relaxed boundary layers which gradually subside as advection becomes the dominant component of the total flux. Such transitional regions do not appear in high Ra cases, where the shift from diffusion to advection is sharp, requiring pronounced, small-scale advection pro-

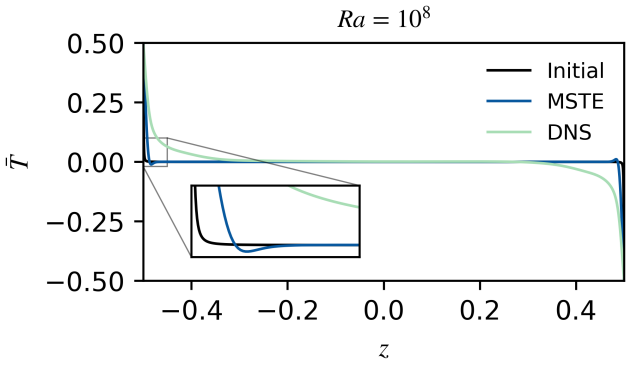

FIG. 2. Mean temperature profiles $\bar{T}$ for $Ra = 10^8$. The initial profile is given by (29). The MSTE curve refers to the mean temperature profile of the marginally-stable thermally-equilibrated state. The DNS profile is obtained by performing a 2-dimensional nonlinear simulation of (1)–(3) with `Dedalus` until thermal and kinetic relaxation. The DNS temperature data are horizontally- and time-averaged. The initial, MSTE, and DNS profiles have increasingly relaxed boundary regions (respectively). The MSTE profile exhibits prominent dips, nested alongside the boundary regions. The source of this feature is not well understood, but similar temperature gradient reversal regions were found by [14] along the midplanes of 2-dimensional convective cellular solutions at $Ra \sim 10^6$.

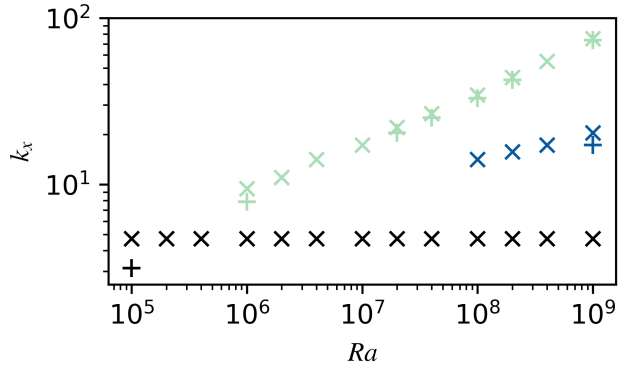

FIG. 3. Wavenumbers of marginally-stable modes of thermally equilibrated states. Markers are color-coded according to their adjacent local maxima index in the eigenvalue spectrum. For example, the spectrum corresponding to $Ra = 10^5$ has adjacent marginal wavenumbers $k_x = \pi, 1.5\pi$. The $Ra = 10^9$ spectrum, shown in lower right corner of Figure 4, has three groups of maxima, with a single marginal mode in the first group ($k_x = 1.5\pi$), two adjacent marginal modes in the second group ($k_x = 6\pi, 6.5\pi$), and two adjacent marginal modes in the third group ($k_x = 23.5\pi, 24\pi$). The largest wavenumbers of the green branch obey a power-law relationship with Ra

files belonging to modes adjacent to the third presumed local maximum in the eigenvalue spectrum. Traversing towards the midplane of the domain, we see increasingly thicker advection profiles corresponding the wavenumbers adjacent to the second local maximum, eventually culminating in the dominant $k_x = 1.5\pi$ mode.

Thermally equilibrated states with large Ra tend to have a more diverse set of marginal modes as compared to small Ra states. In every case, the $k_x = 1.5\pi$ mode is included and is often unaccompanied by adjacent modes. In Figure 3 we give the wavenumbers k_x of marginal modes, color coded accordingly to their respective adjacencies. Marginal modes often appear in neighboring pairs, in which case the larger mode is denoted with an x and the smaller mode is denoted with a +. In these cases we infer the existence of a local maximum eigenvalue between the two adjacent marginally-stable modes. For $Ra \geq 10^6$, a second branch of marginal modes is introduced as shown in green, increasing according to some power-law with respect to Ra. The introduction of this largest branch is likely required to oppose the diffusion of the thinning boundary layers. For $Ra \geq 10^8$, a third branch appears (shown in blue), splitting the widening gap between the blue branch and the green branch. This development is associated with relatively thick advection profiles, filling a niche in the total flux by uniting the sharp profiles of the largest branch (green) and those of the bulk-domain-oriented smallest branch (blue).

In general, marginally-stable thermal equilibria can be characterized by their boundary layer thicknesses, from which, the rest of their properties follow. Letting the interior boundary layer threshold be the z-coordinate at which $\frac{\partial \bar{T}}{\partial z} = 0$, we find that $Ra \propto \delta^{-3}$ as illustrated in Figure 7. This is consistent with Malkus' classical marginal-stability theory, a scaling argument which perceives the boundary regions as subdomains which are themselves marginally-stable.

The Nusselt number, which describes convective performance, is given by

$$\mathrm{Nu} = \frac{\langle A^2 \langle w'T' \rangle_x - \mathcal{P} \frac{\partial \bar{T}}{\partial z} \rangle_z}{\langle -\mathcal{P} \frac{\partial \bar{T}}{\partial z} \rangle_z}. \tag{24}$$

There is no general consensus surrounding the scaling behavior $\mathrm{Nu} \sim Ra^\beta$ for high Ra systems. The asymptotic value of β is of particular importance in astrophysical systems. In Figure 5 we report Nu for MSTE, DNS, along with several ECS. The marginally-stable thermally-equilibrated states and numerical simulation data exhibit power-law relationships with Ra. More specifically, $\beta = 1/3$ which agrees with Figures 7, 3, and 6 and the scaling argument given by [4]. The nonlinear solutions, which maximize heat flux, are obtained by [11]. Nu of both equilibria exceed that of simulations, which might be due to the transitional behaviors outlined by [15] and [16] inhibiting heat flux. Alternatively, we might anticipate the existence of exact coherent states with smaller Nu, forming another node in the Markov chain whose long-term behavior agrees with the simulation data.

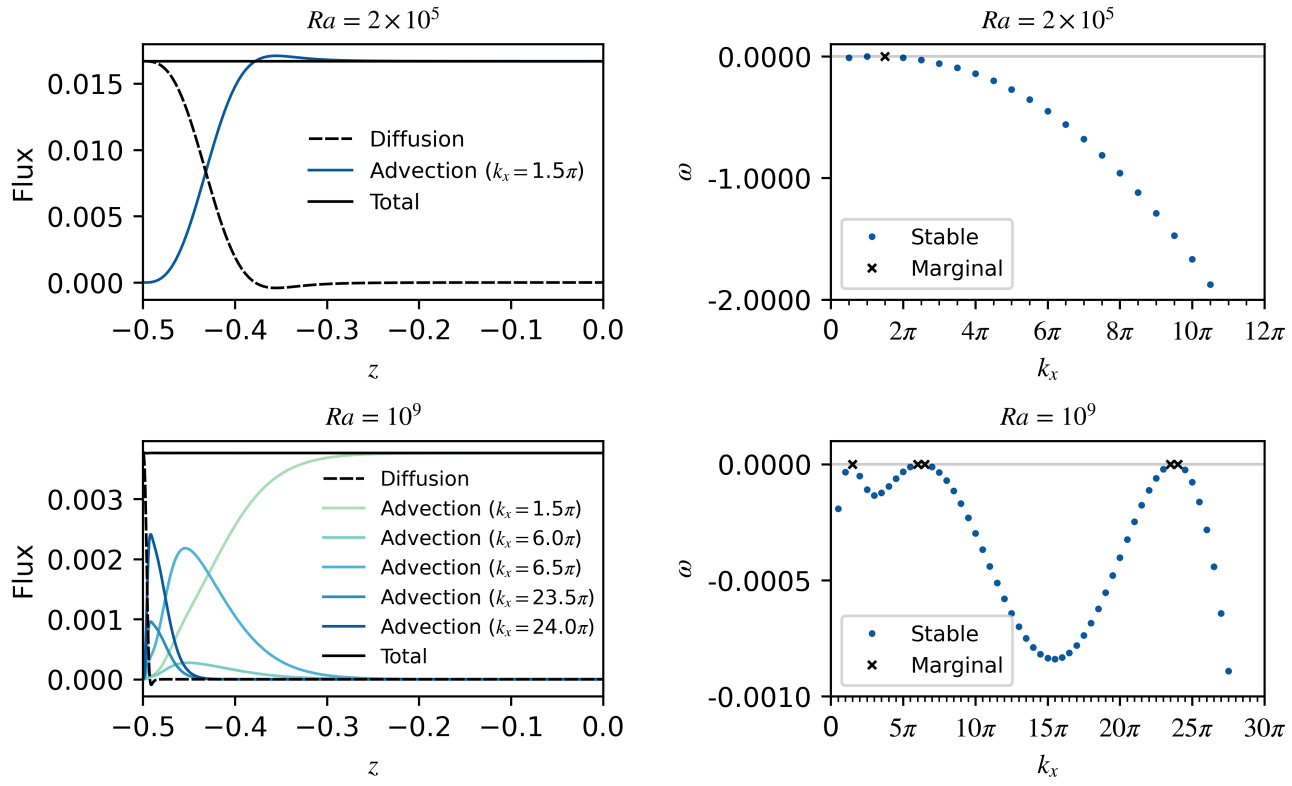

FIG. 4. Heat fluxes (left) and eigenvalue spectra (right) of equilibrated states $Ra = 2 \times 10^5$ (top) and $Ra = 10^9$ (bottom). Advection profiles belong to marginally-stable modes. For low Ra, a single mode with $k_x = 1.5\pi$ is sufficient to oppose boundary layer diffusion and facilitate heat flux throughout the bulk of the domain. For large Ra, high-wavenumber modes contribute pronounced small-scale advection profiles which tightly hug the thin boundary layers. A combination of of progressively wider advection profiles is necessary to transition to the $k_x = 1.5\pi$ mode.

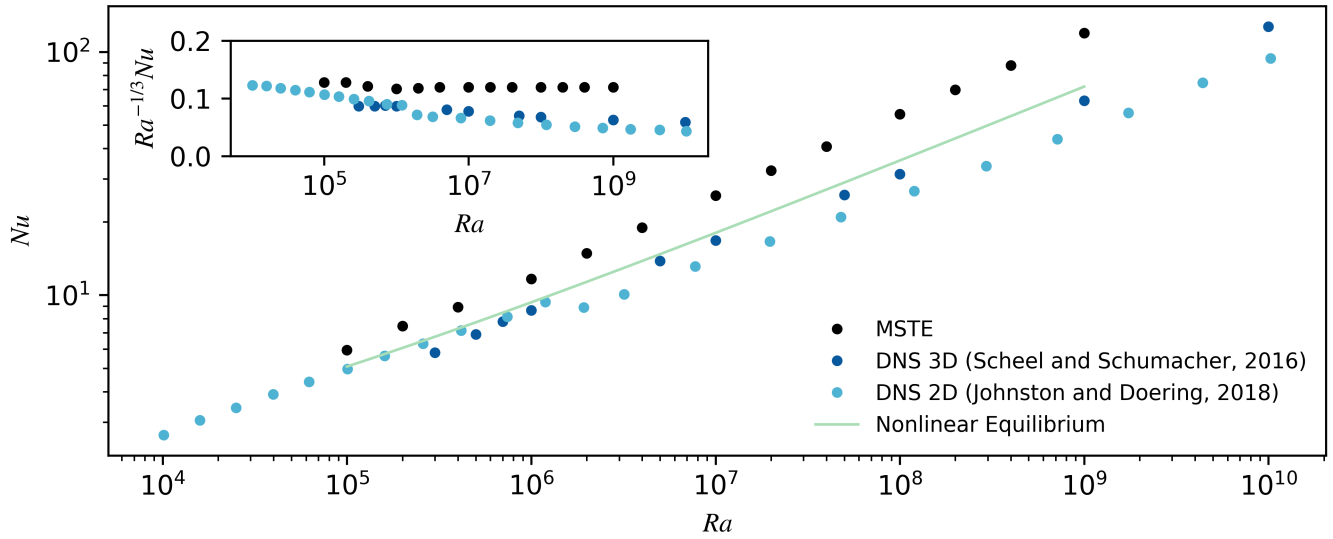

FIG. 5. Nusselt numbers are shown for marginally-stable thermally-equilibrated states, statistically-steady direct numerical simulations performed with `Dedalus` [19], and equilibrated nonlinear solutions, which maximize heat flux, given by [11]. Both obey power-law relationships with Ra, with $\mathrm{Nu} \sim Ra^{1/3}$ in agreement with Figures 7, 3, and 6 as well as [4]. Marginally-stable states' Nusselt numbers exceed simulation Nusselt numbers. This can be explained by the contrasting boundary region geometries shown in Figure 2.

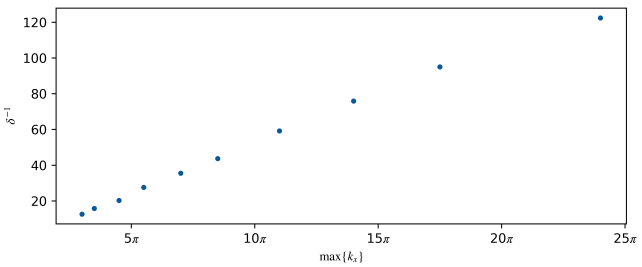

FIG. 6. For $Ra \geq 10^6$, the maximum marginally-stable wavenumber (corresponding to the green X markers in Figure 3) are inversely related to the boundary layer thicknesses δ. $(\max\{k_x\})^{-1}$ gives a minimum x length scale for the perturbations, and consequently, the advection. We expect the minimum z length scale to agree with the boundary layer thickness δ because otherwise the boundary layer would continue to diffuse. This is illustrated in the lower left corner of Figure 4, where the advection profile for $k_x = 24\pi$ is tightly flanked by the surrounding boundary layers. This suggests that the minimum x and z length scales obey some constant ratio.

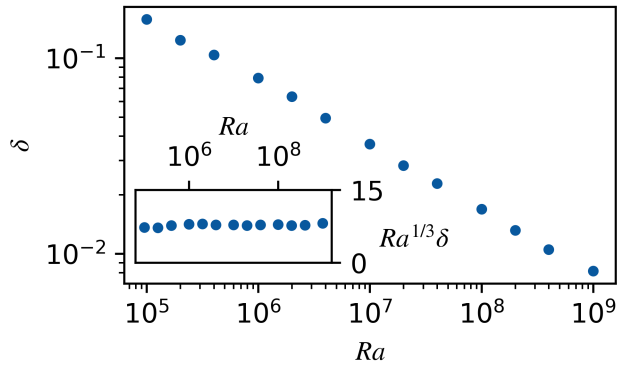

FIG. 7. Boundary layer widths δ of marginally-stable thermal equilibria. We define the threshold of each boundary layer as the z-coordinate at which $\frac{\partial \bar{T}}{\partial z} = 0$, corresponding to the local extrema of the equilibrated curve in Figure 2. Plotting on a log-log scale, we find δ and Ra obey a power-law relationship. We also demonstrate that $Ra^{1/3}\delta$ is approximately constant with respect to Ra implying $Ra \propto \delta^{-3}$, as predicted by [4]

V. SIMULATIONS WITH THERMALLY EQUILIBRATED INITIAL CONDITIONS

This investigation is partially motivated by the prospect of decreasing nonlinear simulation relaxation times by employing thermally-equilibrated initial conditions. Conventionally, (1) - (3) are solved via direct numerical simulation (DNS) with the linear initial conditions

$$T(x,z)\big|_{t=0} = 0.5 - z \tag{25}$$
$$\mathbf{u}(x,z)\big|_{t=0} = \mathbf{0} \tag{26}$$
$$p(x,z)\big|_{t=0} = 0. \tag{27}$$

t in this section now refers to the simulation time as opposed to the thermal equilibration time parameter used previously. We define the MSTE initial conditions

$$T(x,z)\big|_{t=0} = \bar{T}_{\mathrm{MSTE}}(z) + \sqrt{2}\sum_{n=1}^{N} A_n \ \mathrm{Re}\Big[\theta_n(z)e^{ik_{x_n}x}\Big]$$
$$\mathbf{u}(x,z)\big|_{t=0} = \sqrt{2}\sum_{n=1}^{N} A_n \ \mathrm{Re}\Big[\Big(U_n(z)\hat{x} + W_n(z)\hat{z}\Big)e^{ik_{x_n}x}\Big]$$
$$p(x,z)\big|_{t=0} = \sqrt{2}\sum_{n=1}^{N} A_n \ \mathrm{Re}\Big[P_n(z)e^{ik_{x_n}x}\Big] \tag{28}$$

Where $\theta_n(z), U_n(z), W_n(z), P_n(z)$; A_n; and k_{x_n} refer to the complex eigenfunctions, amplitude, and wavenumber at the nth marginal mode respectively. The $\sqrt{2}$ factor is necessary for eigenfunction normalization.

Simulations launched with MSTE initial conditions do not exhibit a convective-transient period, as the large-scale anatomy of convective cells, which are characteristic of Rayleigh-Bénard convection, exist on initialization. This is illustrated in Figure 8, where the sharp spike in Nu is associated with a turbulent transitional period of upwelling until the distinctive plume-like structure is established. Simulation of this transitional period is prohibitive [20]. For high Ra experiments, researchers often "bootstrap" data by initializing simulations with the results of similar Ra runs [21, 22]. MSTE can be perceived as a set of initial conditions, designed for avoiding the simulation of transitional high Reynolds number flows.

MSTE are laminar, lacking the small-scale structures associated with moderate to high Ra experiments. The absence of chaotic dynamics is an apparent consequence of the quasilinear assumptions. If we treat MSTE as background states, DNS suggest that plumes, vortex sheets, and other unstable turbulent features inhibit total heat transfer. This perspective agrees with convectional models of transitions to turbulent flows, such as Boussinesq's turbulent-viscosity hypothesis [23], where the emergence of small-scale velocity structures tends to increase total shear [24–26], thereby impeding buoyancy-driven flows and decreasing advection in the bulk of the domain. We could also atribute the diffuse DNS temperature profile in Figure 2 with unsteady boundary-layer penetration and mixing that MSTE do not exhibit.

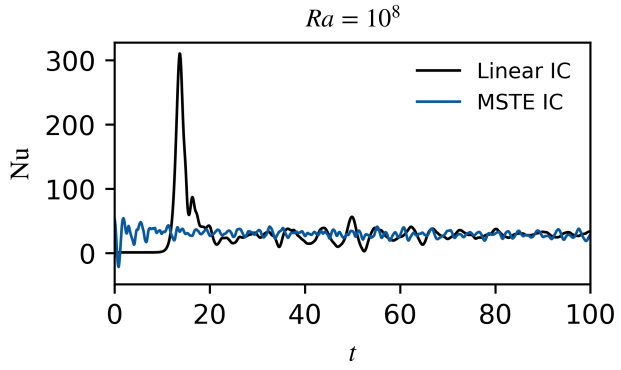

FIG. 8. Nusselt numbers of simulations performed at $Ra = 10^8$ with the conventional initial conditions (black) and MSTE initial conditions (blue). MSTE simulations do not undergo a convective-transient period because the characteristic large-scale convective cell structure exists on initialization. For high Ra simulations, researchers often choose to recycle the results of similar Ra runs [21, 22] because the high-Reynolds number flows associated with the convective transient period are computationally prohibitive [20].

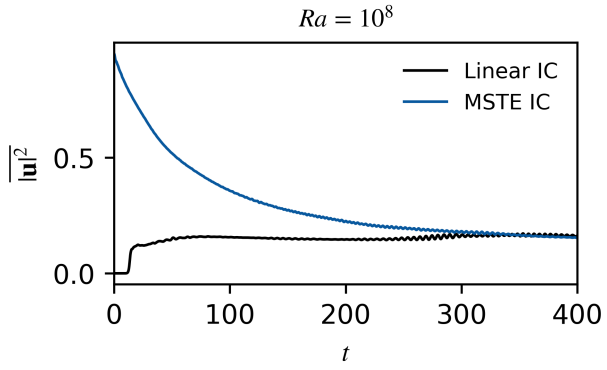

FIG. 9. Average kinetic energies of the same simulations performed in Figure 8 ($Ra = 10^8$). The combination of eigenfunctions which give thermal equilibrium have significantly more kinetic energy than the statistically steady state. Kinetic equilibrium is achieved according to the viscous timescale $t_\nu \sim \sqrt{Ra/Pr}$.

The marginally-stable equilibria are associated with a combination of eigenfunctions whose average kinetic energy is significantly larger than the statistical steady state, as given by Figure 9. This is postpones kinetic relaxation because the large horizontal flows decay on a viscous timescale

$$t_\nu \sim \sqrt{\frac{Ra}{Pr}}.$$

Consequently, marginally-stable thermally-equilibrated initial conditions do not reduce the simulation time required to achieve a statistically steady state, rather, they increase it considerably. Further, this suggests that the MSTE background state perspective is, at least partially, flawed as an appropriate background state would approximate $\langle|\mathbf{u}|^2\rangle_{\mathcal{D}}$

VI. DISCUSSION

In general, the reduced model we study in this paper can be perceived as a unique way to describe Rayleigh–Bénard convection. Solutions to the quasilinear problem retain several key features that are ubiquitous in experiments and simulations: power-law Nu scaling, plume-like structures, and minimum length-scale approximations [4]. They also exhibit unique and unexpected features: gradient-reversal/dips in temperature profiles, kinetic exaggeration, and greater Nu than other time-invariant solutions. We also obtain indistinguishable solutions despite initializing with various mean temperature profiles $\bar{T}(z, 0)$. Thus solutions might be unique, but we cannot demonstrate this rigorously.

As previously noted, solving the EVP for statistically steady DNS data yields positive eigenvalues; the system is in a perpetual state of instability. Unstable modes tend to stabilize the system rapidly, creating a negative feedback loop whose average state is linearly unstable. We might curtail the disagreement between MSTE and DNS by loosening our marginal-stability criterion. Should the time-scales not be entirely separate, we might anticipate the long-term persistance of nearly-marginal unstable modes. This perpetual linear instability cannot be described by our model independently (we do not know, a priori, how unstable such modes are) but it might prove fruitful to investigate moderately unstable thermal equilibria (MUTE). More precisely, instead of traversing the manifold of marginally-stable states toward MSTE, we could consider the manifold of states whose maximum eigenvalue(s) $\omega_{\max}$ agree with some other stability constraint. Note that under this definition, 2-dimensional ECS and temporally-averaged steady DNS data are subsets of MUTE, since they are thermally-equilibrated and generally unstable, though they need not necessarily satisfy the quasilinear form.

We cannot use our reduced quasilinear model to predict Nu $\sim Ra^\beta$ for large Ra without some complementary stability constraint. The eigenvalues of DNS data might provide an informative stability constraint (we could find MUTE and compare them with DNS data), but this would be self-defeating in general. Instead we seek to combine reduced models to approximate β without DNS. Under the marginal-stability constraint, we found that MSTE exhibit classical Malkus scaling, having marginally-stable boundary layers with $\beta = 1/3$. We could instead require that the eigenvalues of MUTE agree with the eigenvalues of the analytic 1-dimensional boundary layer predictions of [27, 28] (which remain in development), allowing us to refine and ex-

pand these estimates into 2-dimensional MUTE. Accessible MUTE states would not rely on DNS, satisfying only the quasilinear problem and stability constraint. Such MUTE ought to agree with DNS data more precisely then MSTE, ideally having less extreme velocities. This is reasonable to expect, since accurate boundary layer approximations and DNS data should have similar stability characteristics. By definition, $\bar{T}_{\mathrm{MUTE}}$ is unstable and would therefore admit more diffuse boundary layer structures, requiring smaller $A^2(t)$ (less advection) to satisfy the stability constraint and thereby reducing Nu, $\langle\langle|\mathbf{u}|^2\rangle_x\rangle_z$ and possibly β.

APPENDIX

A. Initial buoyancy profile

We initialize the thermal-equilibration algorithm with [27]'s analytical thermal boundary layer equation for turbulent Rayleigh-Bénard convection, given by

$$\bar{T}_0(\xi) = \frac{\sqrt{3}}{4\pi}\log\frac{(1+a\xi)^3}{1+(a\xi)^3} + \frac{3}{2\pi}\arctan\left(\frac{4\pi}{9}\xi - \frac{1}{\sqrt{3}}\right) + \frac{1}{4}$$
$$\xi = \frac{z}{\delta_0}, \qquad a = \frac{2\pi}{3\sqrt{3}} \tag{29}$$

where δ_0 is the boundary layer thickness. We expect that each Ra is associated with a unique δ_0 for which $\bar{T}_0(z)$ is marginally-stable. It should be noted that when experimenting with various initial profiles ($\tanh, \mathrm{erf}$, etc.), we obtain indistinguishable equilibrated states, implying that solutions may be unique. An example of (29) is given by the blue curve in Figure 2.

ACKNOWLEDGMENTS

The authors thank Jeff Vassil, Greg Chini, Emma Kaufman for their valuable feedback and suggestions. We also thank the `Dedalus` and `Eigentools` development teams. Computations were performed on the NASA Pleiades system.

[1] L.-A. Couston, D. Lecoanet, B. Favier, and M. Le Bars, Phys. Rev. Research **2**, 023143 (2020).
[2] X. Zhu, V. Mathai, R. J. Stevens, R. Verzicco, and D. Lohse, Physical Review Letters **120** (2018), 10.1103/physrevlett.120.144502.
[3] M. Ossendrijver, Astronomy & Astrophysics Reviews **11**, 287 (2003).
[4] W. V. R. Malkus, Proceedings of the Royal Society of London. Series A, Mathematical and Physical Sciences **225**, 196 (1954).
[5] L. N. Howard, in *Applied Mechanics*, edited by H. Görtler (Springer Berlin Heidelberg, Berlin, Heidelberg, 1966) pp. 1109–1115.
[6] R. H. Kraichnan, Physics of Fluids **5**, 1374 (1962).
[7] E. A. Spiegel, Journal of Geophysical Research **67**, 3063 (1962).
[8] B. Castaing, G. Gunaratne, L. Kadanoff, A. Libchaber, and F. Heslot, Journal of Fluid Mechanics **204**, 1 (1989).
[9] S. GROSSMANN and D. LOHSE, Journal of Fluid Mechanics **407**, 27–56 (2000).
[10] G. Ahlers, S. Grossmann, and D. Lohse, Rev. Mod. Phys. **81**, 503 (2009).
[11] F. Waleffe, A. Boonkasame, and L. Smith, Physics of Fluids **27**, 051702 (2015).
[12] D. Sondak, L. M. Smith, and F. Waleffe, Journal of Fluid Mechanics **784**, 565 (2015), arXiv:1507.03151 [physics.flu-dyn].
[13] B. Wen, D. Goluskin, and C. Doering, (2020).
[14] G. P. Chini and S. Cox, Physics of Fluids **21**, 083603 (2009).
[15] G. Yalnız, B. Hof, and N. Burak Budanur, arXiv e-prints , arXiv:2007.02584 (2020), arXiv:2007.02584 [physics.flu-dyn].
[16] P. Cvitanović and J. Gibson, Physica Scripta **2010**, 014007 (2010).
[17] C. Beaume, G. P. Chini, K. Julien, and E. Knobloch, Physical Review E **91** (2015), 10.1103/physreve.91.043010.
[18] G. Michel and G. P. Chini, Journal of Fluid Mechanics **858**, 536–564 (2019).
[19] E. H. Anders, G. M. Vasil, B. P. Brown, and L. Korre, Phys. Rev. Fluids **5**, 083501 (2020).
[20] E. H. Anders, B. P. Brown, and J. S. Oishi, Phys. Rev. Fluids **3**, 083502 (2018).
[21] R. Verzicco and R. Camussi, Physics of Fluids **9**, 1287 (1997), https://doi.org/10.1063/1.869244.
[22] H. Johnston and C. R. Doering, Phys. Rev. Lett. **102**, 064501 (2009).
[23] J. Boussinesq, (1877).
[24] D. Lecoanet, M. McCourt, E. Quataert, K. Burns, G. Vasil, J. Oishi, B. Brown, J. Stone, and R. O'Leary, Monthly Notices of the Royal Astronomical Society **455**, 4274 (2016), publisher Copyright: © 2015 The Authors.
[25] P. G. Drazin and W. H. Reid, *Hydrodynamic Stability*, 2nd ed., Cambridge Mathematical Library (Cambridge University Press, 2004).
[26] S. B. Pope, *Turbulent Flows* (Cambridge University Press, 2000).
[27] O. Shishkina, S. Horn, S. Wagner, and E. S. C. Ching, Phys. Rev. Lett. **114**, 114302 (2015).
[28] X. Zhang, D. P. M. van Gils, S. Horn, M. Wedi, L. Zwirner, G. Ahlers, R. E. Ecke, S. Weiss, E. Bodenschatz, and O. Shishkina, Phys. Rev. Lett. **124**, 084505 (2020).